Restoration of distorted images, terahertz generation and terahertz interference based on multiple-coupled optical parametric oscillators

Yujie J. Ding*
Department of Electrical and Computer Engineering
Center for Photonics and Nanoelectronics
Lehigh University, Bethlehem, PA 18015, USA

**Corresponding author: yding300@gmail.com*

Abstract

We review our progress made on applications of coupled optical parametric oscillators based on a composite consisting of adhesive-free-bonded $KTiOPO_4$ stacks. By using the phase-conjugate output generated by the composite, we have demonstrated that the spatial profile after the beam propagates through the phase-distorted medium can be restored to the profile before the distortion. In addition, we have restored the images being blurred by the phase distortion. We have efficiently generated terahertz outputs by mixing the idler twins from the coupled optical parametric oscillators. By using the alternatively-rotated GaP plates as an output coupler for the coupled optical parametric oscillators, we have efficiently generated terahertz waves based on an intracavity configuration. By placing both the composite and a bulk $KTiOPO_4$ crystal in the same cavity, we have demonstrated the interference effect of the THz waves generated by using different pairs of the optical beams.

Number of our report according to workshop program: 1.13.1
Topic: Interaction of Laser Radiation with Matter
PACS: 42.65.Ky, 42.65.-k, 42.65.Re
Keywords: Coupled optical parametric oscillators, restoration of blurred images, phase conjugation, coupled parametric processes, difference-frequency generation, nonlinear-optical materials, terahertz sources, terahertz interference.

I. Introduction

A coherent infrared source being capable of generating dual wavelengths have a variety of applications such as differential absorption lidar [1], Doppler lidar measurement [2], coherent anti-Stokes Raman scattering microscopy [3], and generation of mid-infrared [4] and terahertz (THz) [5] waves. Although a conventional optical parametric oscillator (OPO) is capable of generating signal and idler wavelengths, spatial walk-off in a nonlinear crystal not only increases the threshold for the oscillation but also sacrifices the beam quality. Previously, it was demonstrated that periodically-orientated $KTiOPO_4$ (KTP) stacks based on adhesive-free-bonding (AFB) can be used to compensate spatial walk-off for the generation of about 2 μm due to quasi-phase-matching (QPM) [6]. In comparison, conventional QPM crystals have very small aperture sizes. Besides, compared with two separate nonlinear optical crystals [4,5], such a crystal composite has a significantly higher gain, i.e. a factor of $16/\pi^2$ higher [6]. In addition, because the dual-signal or dual-idler wavelengths (i.e. four output wavelengths) are generated simultaneously inside the same crystal, each pair has almost the same intensity and the temporal profiles which are completely synchronized.

Using a pump beam at the wavelength of 532 nm, singly resonant OPO's were implemented based on the AFB KTP stack composite [7]. Such coupled OPO's have a threshold pump power which is more than four times lower than that based on a single KTP crystal. Using the idler twins from such OPO's, we efficiently generated THz waves [7]. Besides THz generation, such a configuration allows us to restore the images being blurred by phase distortion based on phase conjugation [8]. In the past, phase-conjugation devices based on photorefractive effect had response times in the range of 100 μs – 1 s [9], i.e. they were extremely slow. Obviously, such response times make the corresponding scheme impracticable for compensating the blurred images due to atmospheric turbulence. It is well known that four-wave mixing in a third-order nonlinear medium can be used to achieve optical phase conjugation [10]. However, this scheme requires two pump beams. What is more, since third-order nonlinearity is weak, the pump powers must be extremely high in order to achieve a reasonably high nonlinear power reflection coefficient, i.e. nonlinear reflectivity (e.g. $R_{pc} \geq 1\%$). In comparison, our novel approach realized in Ref. [8] has the temporal response time being limited only by the propagation time of the interacting beams. Moreover, it is based on a second-order nonlinear process, which is much stronger than the third-order nonlinear process. Therefore, our approach overcomes the disadvantages of the slow response and the requirement of high pump intensities.

It is worth noting that such coupled OPO's have unique advantages. Indeed, frequency separation is insensitive to the fluctuations of pump frequency and temperature. In the past, all of the schemes based on nonlinear processes in the past suffer from a major drawback, i.e. optical phase conjugation works only for a specific polarization and wavelength of the input beam [11-13].

In this article, we summarize our results on the applications of coupled OPO's in corrections of distorted images, THz generation, and observation of the interference of THz waves.

II. Correction of spatial beam profile after phase distortion

In this Section, we summarize our result on the generation of a phase-conjugate beam based on AFB periodically-inverted KTP plates [14]. We have generated a phase-conjugated beam which is insensitive to the polarization of the input beam. We have demonstrated that using the phase-conjugated beam, we can recover the spatial beam profile after phase distortion.

A composite KTP stack has 20 pieces of x-cut KTP plates with the cutting angles of $\theta = 90^{\circ}$ and $\varphi = 0^{\circ}$, indicating that each plate is noncritically phasematched. As the 20 plates were cut from the same bulk KTP crystal, the crystal axes of these plates are aligned to the same directions initially. Before forming the stack, the crystal axes of every other plate are inverted such that the corresponding elements of the second-order nonlinear susceptibility tensor of KTP are all inverted. Such periodic modulations result in a QPM condition [6], i.e. $\Delta k l = \pm\pi$, where Δk is the wave-vector mismatch for each nonlinear parametric process and l is the thickness of each KTP plate. As a result, for each pump wavelength, there is a pair of the signals as well as a pair of the idlers that satisfy the condition above. Each KTP plate has a thickness of 1.19 mm ± 0.01 mm. When the pump wavelength is set to 532 nm, the wavelengths for the pair of the signals are 1034.8 nm and 1044.2 nm (ordinary wave - *o*) whereas those for the pair of the idlers are 1084.1 nm and 1093.9 nm (extraordinary wave - *e*), respectively, as shown in Fig. 1 [7]. As the pump wavelength is increased to 539 nm, the two nonlinear parametric processes reach the degenerate point. However, the wavelengths of the signal and idler are different, i.e. the wavelengths for the first pair of signal and idler are 1073 nm (e) and 1083nm (*o*) whereas the wavelengths for the second pair are 1083 nm (*e*) and 1073 nm (*o*), respectively. In contrast, at the degenerate point in a bulk KTP crystal, the signal and idler have exactly the same wavelength of 1078 nm.

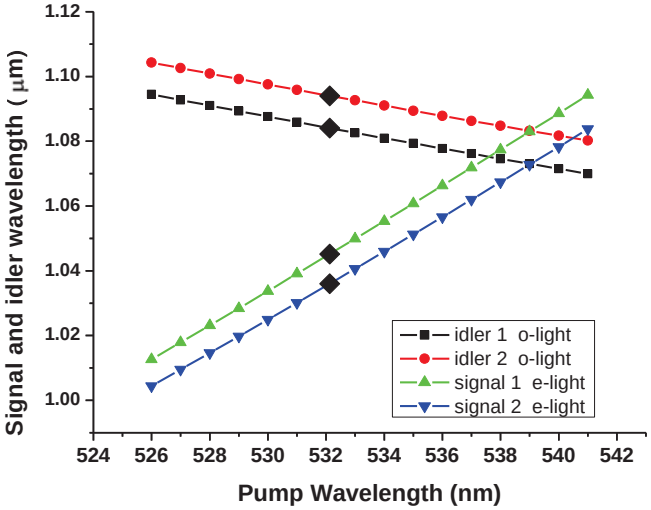

Fig. 1. Signal and idler wavelengths generated from AFB-KTP plates.

The generation of two pairs of the orthogonally-polarized signals and idlers can be exploited for generating the polarization-insensitive phase-conjugated beams. Indeed, assuming that the input beam at 1073 nm has both horizontal and vertical polarization components, the phase-conjugated beams for these two corresponding polarizations can be simultaneously generated by mixing them with the pump beam at 539 nm. Indeed, we mixed the pump beam at 539 nm with the input beam at 1073 nm, polarized in a horizontal or a vertical direction. Fig. 2(a) shows the spectrum for the horizontally-polarized input beam at 1073 nm after mixing it with the pump beam. A phase-conjugated beam in the vertical direction was observed at 1083 nm. Similarly, when we mixed the input beam at 1073 nm, polarized in the vertical direction, with the pump beam,

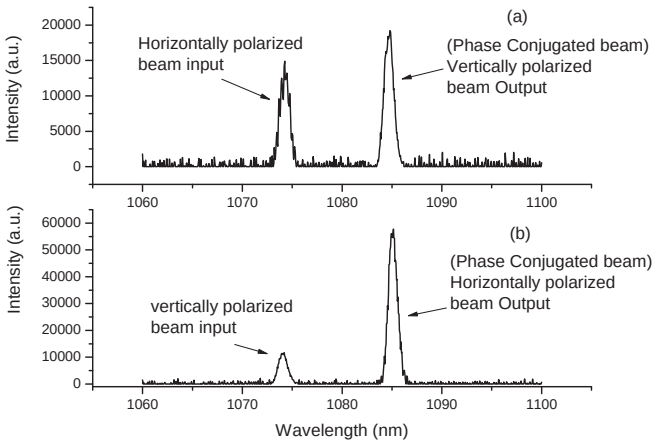

Fig. 2. Polarization-insensitive generation of phase conjugated beam.

the phase-conjugated beam at 1083 nm was observed, which was horizontally polarized, see Fig. 2(b).

In order to demonstrate the restoration of an image being blurred by a turbulent medium based on phase conjugation, we assembled a setup based on the nonlinear parametric processes in the AFB KTP plates, see Fig. 3. The pump beam at 539 nm is an output generated by a MOPO system (10 Hz, 5 ns). In order to generate the input beam for the phase conjugation, we set up an optical parametric oscillator (OPO) based on a bulk KTP crystal. The signal of such an OPO was then used as an input beam and mixed with the pump beam at 539 nm inside the AFB-KTP stack. To simulate a blurred image, a phase-distorting plate was inserted into the optical path. To recover the image from such distortion, the phase-conjugated beam was then reflected back along the previous path by a mirror and it subsequently propagated through the distorting plate at the same spatial location. A CCD camera was used to capture the image being generated by the phase-conjugated and residual input beams, respectively, by switching between the two positions #1 and #2. Correspondingly, the image being captured from position #1 has a significantly-improved image quality compared with that being captured at position #2, see Figs. 4(a) and 4(b).

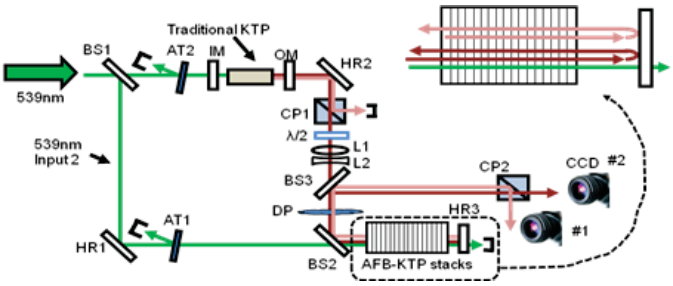

Fig. 3. Experimental setup for the image recovery.

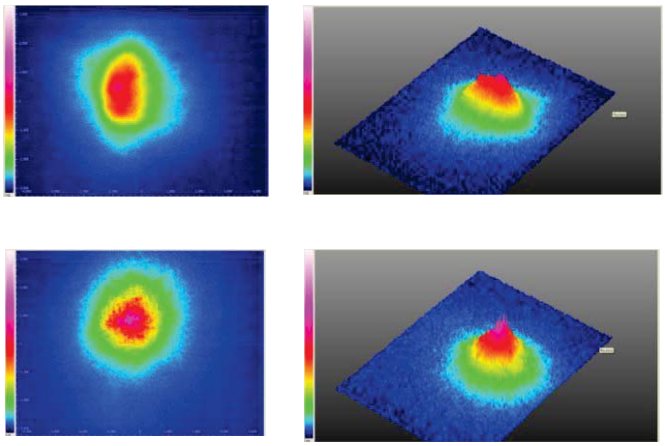

Fig. 4. (a) Spatial profile of phase-conjugated beam; (b) spatial profile of distorted input beam.

III. Restoration of blurred images

In this section, we review our previous experimental result on the restoration of the blurred images caused by the phase distortion [8].

The nonlinear composite used in the parametric interaction consists of 20 pieces of x-cut KTP plates with the cutting angles of $\theta = 90^\circ$ and $\varphi = 0^\circ$. Each plate has a thickness of 1.19 ± 0.01 mm and a cross-section of 5.6 mm×10.5 mm. All 20 pieces are bonded together by AFB technique. Since crystal axes of every other plate are inverted, the signs of nonlinear coupling coefficient d_{eff} are periodically inverted, this periodic alternation the sign of d_{eff} can compensate for the nonzero wave vector mismatch Δk, resulting in the quasi-phase matching (QPM) condition [6,7]. Such a QPM condition causes each pair of the signal and idler in a bulk KTP crystal splitting into two pairs of the orthogonally-polarized signal and idler beams. Therefore, QPM can be used to compensate for the spatial walk-off and allows us to use the largest nonlinear coefficient in the crystal for a nonlinear interaction [6].

Our experimental setup is shown in Fig. 5 for demonstration of image restoration based on broadband and polarization-insensitive phase conjugation. The laser beam (10 Hz repetition, 4.8 ns pulse width) is from an output of Master Oscillator/Power Oscillator (MOPO), with wide range wavelength tenability. The pump beam is split into two parts for each fixed pump wavelength in 535-542 nm. One part is used to pump the optical-parametric oscillator based on a bulk KTP crystal, whereas the other part is directed to the AFB-KTP plates. The idler beam generated from the bulk KTP passes through a cubic polarizer (CP1) and collimated by a pair of convex (L1) and concave (L2) lenses. It then transmits through a phase distortion plate (DP) and used as an input beam for DFG with the green pump beam in the AFB-KTP plates, where temporal and spatial overlaps of the input and pump pulses need to be maintained. Since the DP imposed phase distortion $\varphi(x, y, z)$ on the input signal, the generated phase-conjugate beam from the AFB-KTP plates also has the same phase distortion but with an opposite sign $-\varphi(x, y, z)$. Both the input and generated phase-conjugate beams are reflected back by the high-reflectivity mirror (HR3) and pass through the DP. The input beam suffers the phase distortion of $2\varphi(x, y, z)$ after the second pass of the DP, but for the phase-conjugated beam with the phase distortion of $-\varphi(x, y, z)$, passing through the DP just eliminates the phase distortion and recovers the wave front. Then, the signal and phase conjugate beams are directed to an imaging system by a beam splitter (BS3). The input beam is illuminated on the object and forms a blurring image on the CCD camera because of the phase distortion. While the image formed by the generated phase-conjugate beam will be restored since the phase distortion is removed. The phase conjugate beam has an orthogonal polarization with the input beam. If the input beam is *p*-polarized, it passes through a cubic polarizer (CP2) without reflection, and the generated phase conjugate beam is s-polarized reflecting from the CP2 with an angel ~90°, as shown in Fig. 5. The polarization of the input beam can be tuned by a λ/2 wave plate. The filter in the imaging arm is used to block the remaining green pump beam. By measuring this phase-conjugated beam, we have corrected the blurred images caused by the distortion plate.

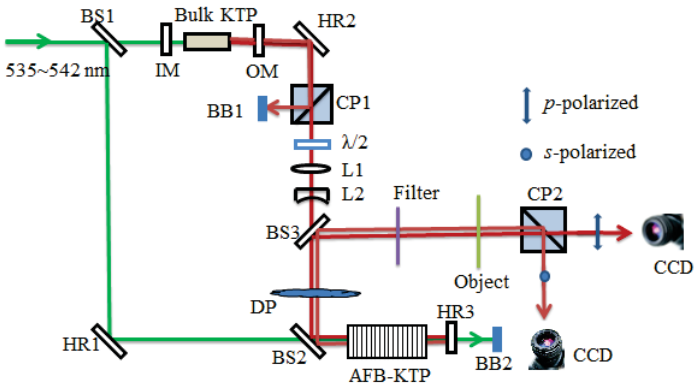

Fig. 5. Experimental setup for imaging based on phase conjugation. BS1-3: Beam splitter; HR1-3: high reflection mirror; IM: input mirror; OM: output mirror; BB1-2: beam block; L1-2: convex and concave lens; CP1-2: cubic polarizer; λ/2: half-wave plate; DP: distortion plate; CCD: CCD camera.

Fig. 6 shows our results of polarization-insensitive restoration of images. The input beam is *p*-polarized for Fig. 6(a) and *s*-polarized for Fig. 6(d) without the phase-distortion plate. After putting in the phase-distortion plate, these images are obviously blurring [Fig. 6(b) and Fig. 6(e)], since the wave front of the input beam is distorted. The phase-conjugated beam can correct the blurred images, and therefore,

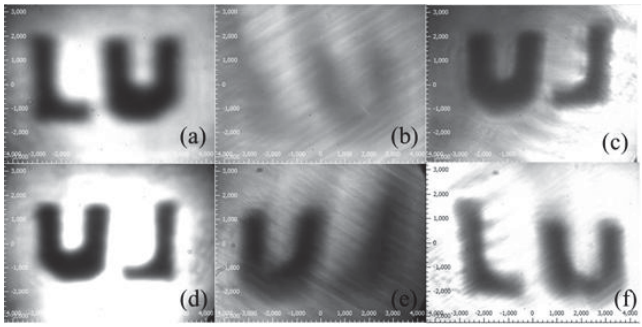

Fig. 6. *P*-polarized (a) and *s*-polarized (d) input beam without distortion images, after distortion images (b) and (e); restored images (c) and (f) by phase-conjugated beams at pump wavelength of 539 nm.

restores the images to the original quality [Fig. 6(c) and Fig. 6(f)]. Based on Fig. 6, we have estimated the degree of the image restoration to be 80±20% with 0% and 100% corresponding to no and complete restorations, respectively.

At around 539 nm pump, two pairs of the signal and idler become degenerate, as shown in Fig. 7(a). Therefore, instead of four different wavelengths, there are only two wavelengths of ~1073 nm and ~1083 nm. Each of these two wavelengths contains both *p*- and *s*-polarized components. Therefore, for the input beam wavelength at (or near) these two wavelengths, phase conjugated beams can be always generated for any polarization. Here, using the AFB-TTP crystal, we demonstrate that the imaging restoration based on polarization-insensitive phase conjugation is not only effective at the region of the degenerate pump point, but also in a broad wavelength range (535 -542 nm).

Fig. 8 shows the imaging restoration at 535 nm, i.e. away from the degenerate pump point. In such a case, the blurred images are also restored by the phase conjugated beams for both *p*-polarized and *s*-polarized input beams. Fig. 8(a) and Fig. 8(d) are the original images without the phase-distortion plate for the *p*-polarized and *s*-polarized input beams respectively. These images become blurring after the distortion plate is placed [Fig. 8(b) and Fig. 8(e)], and restored by the phase-conjugate beams [Fig. 8(c) and Fig. 8(f)]. Two pairs of signal and idler will be generated under the 535 nm pump, as seen the gray region in Fig. 7(a). Two idler beams are *p*-polarized and have wavelengths of ~1080 nm and 1090 nm, while the two signal beams are *s*-polarized and have wavelengths of ~1060 nm and 1050 nm. The polarization of the input beam (~1085 nm) can be tuned by the half-wave plate. If the input beam is *p*-polarized, the output phase conjugate beams are *s*-polarized and have exactly the same wavelength as the signal beams generated in the AFB-KTP crystal, as shown in Fig. 7(b) the blue peaks. Rotate the half-wave plate to make the input beam *s*-polarized, and then the phase conjugated beams become *p*-polarized and have exactly the same wavelengths of idler beams as

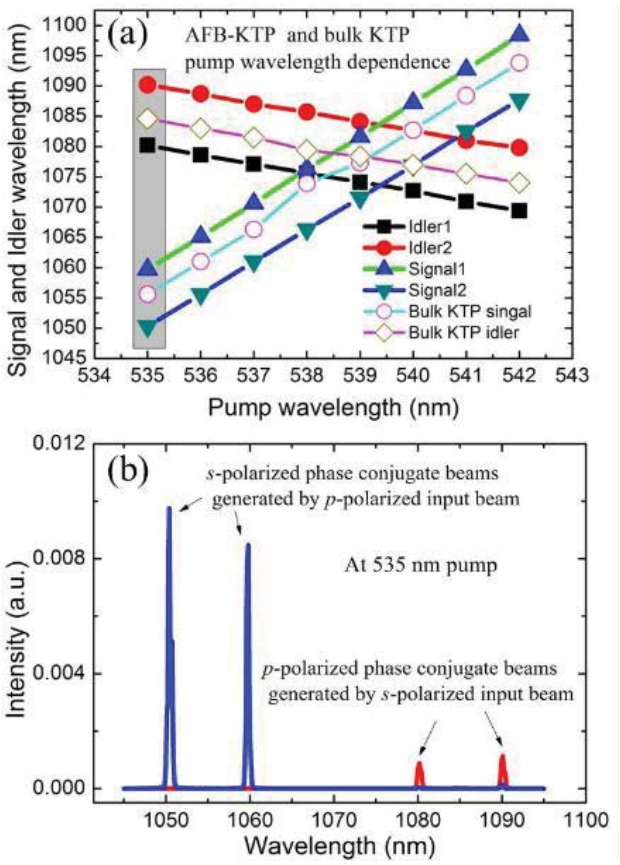

Fig. 7. (a) Measured signal and idler wavelengths of AFB-KTP and bulk KTP as a function of pump wavelength; (b) Phase conjugated beam spectra generated by *p*-polarized input beam (blue peaks) and *s*-polarized input beam (red peaks).

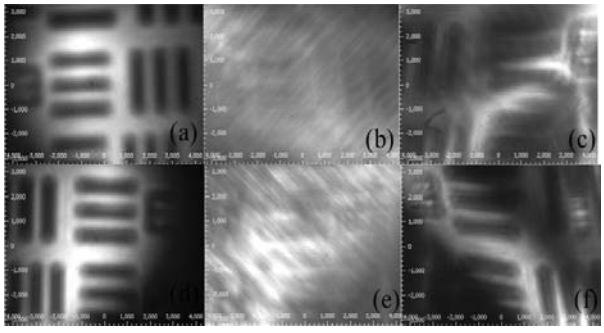

Fig. 8. Image restoration at pump wavelength of 535 nm. *p*-polarized (a) and *s*-polarized (d) input beam without distortion image, after distortion (b) and (e) and restored image (c) and (f) by phase conjugated beams.

shown by the red peaks in Fig. 7(b). It is worth noting that our experiment is different from the previous work on phase conjugation by DFG [6,8]. In their reports, strict restrains are imposed on polarizations and wavelengths of the input beams - only certain polarization direction and wavelength of the input beams can be used for the generation of phase conjugation beams. In contrast, in our case, phase conjugation beams can be generated by either *p*-polarized or *s*-polarized input beams, i.e. it can be generated by the input beam at any polarization direction. Also, this polarization-insensitive phase conjugation can be achieved at broad wavelength range (535 - 542 nm), besides the wavelength at the degenerate pump point (~539 nm). One limitation of our method is that two phase-conjugate wavelengths generated propagate with a very small angle. Therefore, the propagating distance of the phase-conjugate beams needs to be kept as short as possible, before they are divided into two separate beams and illuminate the object and camera.

IV. THz generation using output of coupled OPO's

In this Section, we review our new results on the oscillations at the dual-signal and dual-idler wavelengths of around 1 μm [7]. By mixing the dual-idler output at 1084.1 nm and 1093.9 nm from the coupled OPO's, we generated a THz wave at the wavelength of 118 μm based on difference-frequency generation (DFG).

Each KTP plate was cut according to $\theta = 90^\circ$ and $\varphi = 0^\circ$ (i.e. x-cut). As a result, at these angles the OPO can be noncritical-phase-matched at the pump wavelength of around 532 nm. All the crystal axes of the adjacent plates are opposite to each other in order to periodically switch all elements of second-order nonlinear susceptibility tensor of KTP to realize QPM based on d_{24}. The structure of the KTP plates studied here is quite different from that in Ref. [6]. Indeed, in Ref. [6], z axes of the adjacent KTP plates were bonded in a head-to-tail configuration (i.e. $\theta = 50.2^\circ$) to achieve not only the walk-off compensation but also QPM. It is worth noting that a singly resonant OPO is inherently more stable than a doubly resonant OPO implemented in Ref. [6]. Moreover, the thickness of each KTP plate, dictated by the frequency separation of the dual signals, is different from that in Ref. [6] (i.e. 2 mm).

The experimental setup for the singly-resonant OPO is shown by Fig. 9. The AFB KTP stacks, fabricated at Onyx Optics, consist of 20 x-cut KTP plates, each of which has a thickness of 1.19±0.01 mm, with their z axes being periodically switched as shown by Fig. 9; they were adhesive-free-bonded together as a composite for realizing QPM simultaneously at the dual-signal and dual-idler wavelengths. As a result, the QPM condition is given by $\Delta kl = \pm\pi$, where l is the thickness of each KTP plate. Consequently, a pair of the signals having slightly different wavelengths satisfies the QPM condition above. The two corresponding idler wavelengths satisfy the QPM condition.

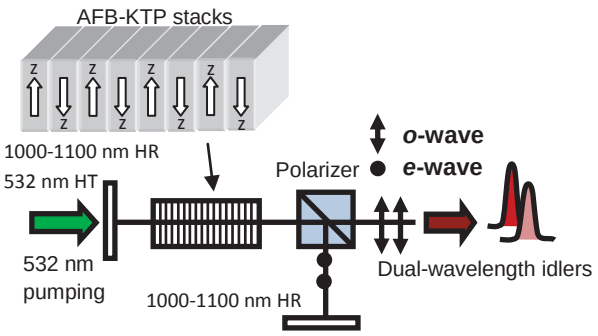

Fig. 9. Experimental setup for singly resonant OPO.

In comparison, only a single signal wavelength satisfies the birefringence-phase matching condition (i.e. $\Delta kl = 0$) if a single KTP crystal is used instead. Our composite has a clear aperture of 5.6 mm×10.5 mm and a total interaction length of 23.8 mm. As one can see, the aperture size is much larger than the QPM KTP crystals commercially available. As a result, such an AFB

crystal composite holds great promise for the generation of high powers, which requires large laser beam sizes. For our composite, both the input and output facets were high-transmission (HT)-coated at the wavelengths of around 532 nm and 1000-1100 nm. To demonstrate the tunability of our OPO based on the KTP composite, we tuned the pump wavelength around 532 nm. Based on our experimental results, low-cost pulsed pump source at 532 nm, commercially available, was sufficient to achieve stable oscillations in the composite. The configuration for the OPO cavity is shown by Fig. 9. Two flat mirrors with high reflection (HR) coating in the range of 1000-1100 nm were designed as the cavity mirrors. To ensure the oscillations only at the signal wavelengths, a cubic polarizer was placed inside the cavity. It allows the o-polarized idler beams to pass through (i.e. $T \approx 97\%$) and reflects almost all of the e-polarized signal beams ($R > 99\%$). Since the polarization of each signal was perpendicular to that of the corresponding idler, we were able to oscillate just the dual signals inside the cavity. Almost all the powers of the dual-idler beams were transmitted through the polarizer. The inset to Fig. 10 illustrates the spectra of the dual signals and dual idlers generated by the OPO at the pump wavelength of 532 nm. The dual signals appearing in the spectra were caused by their weak transmissions through the polarizer. The wavelengths of the dual signals oscillating in the OPO cavity were measured to be 1034.8 nm and 1044.2 nm, whereas the wavelengths of the dual idlers were 1084.1 nm and 1093.9 nm, respectively. These measured wavelengths coincide with the calculated values.

When a pump beam at 532 nm with the repetition rate of 10 Hz and the pulse width of 4.8 ns was slightly focused onto the AFB KTP composite (a beam diameter of about 2 mm, measured by us), we measured the total output power from the OPO vs. the pump power, see Fig. 10. By linearly fitting the data points in Fig. 10, we deduced the threshold power for the OPO to be 12 mW (the corresponding energy of 1.2 mJ per pulse). Such a threshold power corresponds to an intensity of 8 MW/cm^2. At the pump power of 111.8 mW, the OPO output power reached 39 mW, corresponding to a conversion efficiency and slope efficiency of 34.9% and 37.1%, respectively. To demonstrate the advantage of a higher gain in the AFB KTP composite, we measured the power dependence from an OPO based on two traditional KTP crystals which were placed in the setup similar to Ref. [5], see Fig. 10.

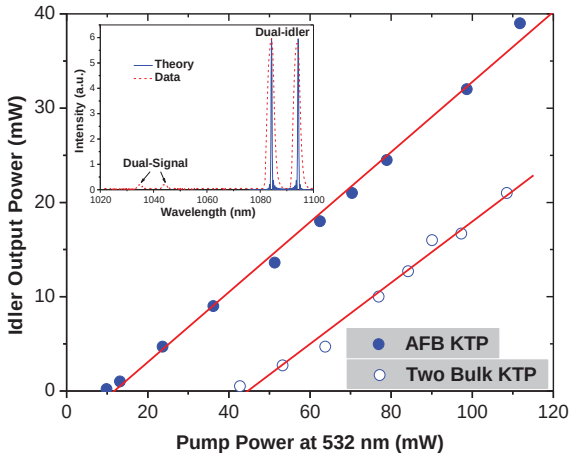

Fig. 10. Average output power of dual-idler beams vs. pump power at 532 nm based on both in AFB KTP and two bulk KTP crystals. Solid lines correspond to linear fits. Inset: spectra of signals and idlers generated by AFB KTP OPO.

Each of the two KTP crystals generated a pair of signal and idler at the slightly different wavelengths of around 1 μm. The length of each crystal is 10 mm such that the total length is 20 mm, which is close to the length of the AFB KTP. At the pump power of 108.5 mW, the dual-idler output power was 21 mW which was 53.8% of the output power generated from AFB KTP. This value is close to an estimate of 42.8%, considering the slightly length difference between the AFB KTP composite and two traditional KTP crystals. Since the implemented OPO is singly resonant, the spectrum and power of the dual-idler beams are rather stable based on our observation.

By mixing the dual-idler beams from the OPO based on DFG [15-17] in four-piece alternatively-rotated GaP plates, we generated the THz wave based on the setup shown by Fig. 11. Each GaP plate cut along the (110) plane had a thickness of 663 μm. The polarizations of the dual-idlers were along the same direction, which is different from the condition in Refs. [15,16]. As we rotated the azimuthal angle of a single GaP plate, the THz intensity exhibited a unique dependence, see Fig. 12. This is caused by the dependence of the second-order nonlinear coefficient on the polarization directions of the mixing beams relative to the azimuthal angle of the plate. Considering the above conditions and cut angle of GaP plate, the THz intensity can be shown to be $\propto \cos^4(\varphi)+\sin^2(2\varphi)$, where φ is the azimuthal angle, see Fig. 11. From Fig. 12, the measured data agree quite well with the theoretical values. We measured the THz power generated by the four-piece alternatively-rotated GaP stacks vs. the average power of the dual idlers from the OPO, see Fig. 13. At 37.2 mW, the THz peak power was measured to be 40.8 W. We fitted the data points using a quadratic dependence, which corresponds to the solid curve in Fig. 13. Obviously, the measured data clearly exhibit a quadratic dependence which is the typical characteristics of DFG. Based on the data presented in Fig. 13 the THz output power is stable.

By scanning a Si-based etalon, THz wavelength was measured to be 121 μm, which agrees well with the designed value of 118 μm (see inset to Fig. 12).

The THz frequency is determined by not only the phase-matching condition of the pump, signal and idler from the OPO's, but also the QPM condition due to the presence of the alternatively-inverted AFB KTP plates. The THz output frequency is given by $\nu_{THz}=\nu_{i1}-\nu_{i2}$, where ν_{i1} and ν_{i2} are the frequencies of the idler beams generated by the OPO. Since the pump wavelength of the OPO is 532 nm, the THz frequency is calculated to be 2.55 THz, which is close to 2.54 THz (118 μm). In addition, to explore the tunability of the THz generation, we varied the pump wavelength

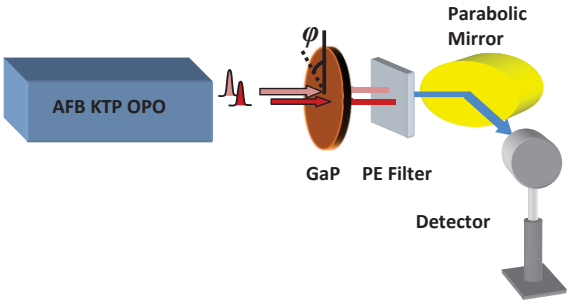

Fig. 11. An experimental setup for THz generation.

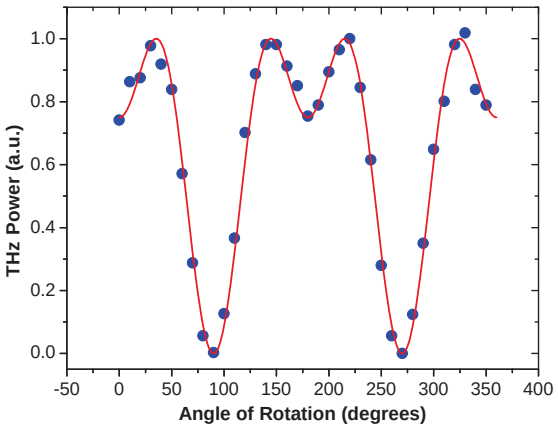

Fig. 12. THz power as a function of azimuthal angle in GaP plate. Dots correspond to experimental results. Solid curve corresponds to theoretical result.

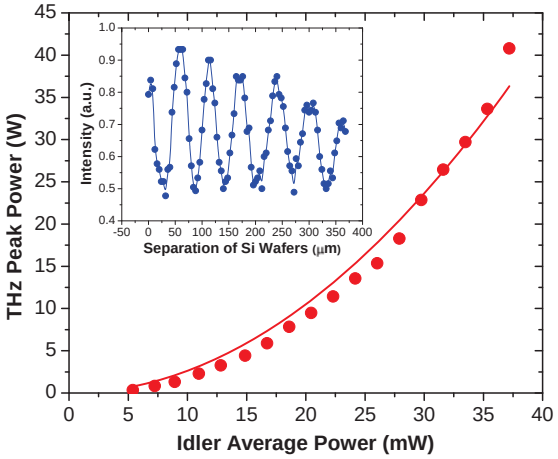

Fig. 13. Dependences of THz peak power on the dual-idler average power emitted from the OPO. Solid curve corresponds to the quadratic fit. Inset: the power being transmitted through a Si-based etalon versus the distance.

within the range of 512-552 nm. Fig. 14 illustrates the tuning characteristics. According to Fig. 14, the THz output wavelength can be tuned in the range of 105.0-133.7 μm, corresponding to the frequency range of 2.244-2.857 THz.

V. THz intracavity generation

In Section, we summarize our result on THz generation based on intracavity difference-frequency generation in stacked GaP plates as an output coupler of an optical parametric oscillator [18]. The total THz output peak power approaches 200 W.

In order to reach the QPM condition for the OPO's, let us consider the THz generation outside t he OPO cavity, shown in Fig. 15. This is similar to that in Ref. [7] except that the dual-signal beams are used for the THz generation. In such a case, the GaP plates were placed in the arm of the dual-wavelength signals which have the polarizations being perpendicular to that of the pump and idler beams. A cubic polarizer was placed in the cavity such that only the dual signal waves were reflected. Therefore, the damage of the KTP plates by the pump beam can be avoided. Before achieving the intracavity frequency conversion, we optimized the pump wavelength by using the external-cavity scheme shown by see Fig. 15. Different from the setup in Ref [7], the dual-idler beams were confined inside the OPO cavity while the dual signals were the output beams. Another key component inside the cavity is the adhesive-free bonded KTP plates, consisting of 20 pieces (each has its thickness of 1.19 mm), which were used as a gain medium for the OPO. It has a clear aperture of 5.6 mm × 10.5 mm and a total interaction length of 23.8 mm. Due to quasi-phase-matching (QPM), a single pair of the signal and idler in a bulk KTP crystal was split into two pairs of the signals and idlers (i.e. totally four output wavelength wavelengths) [6].

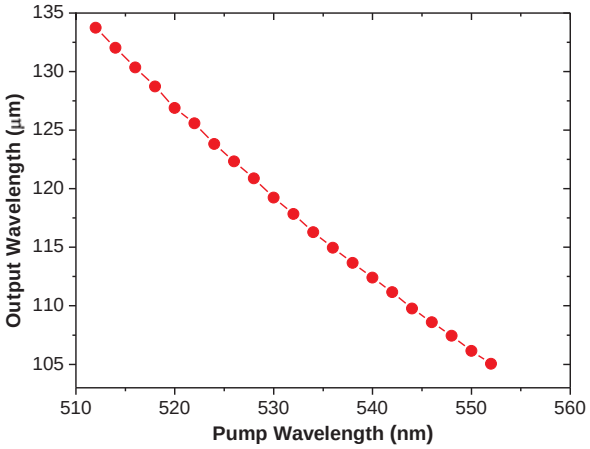

Fig. 14. An illustration of the tuning characteristics.

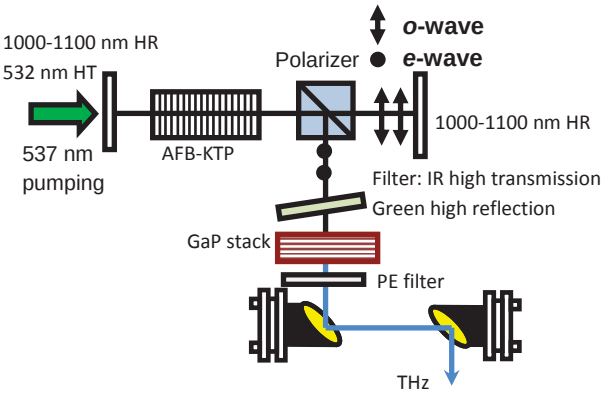

Fig. 15. Experimental setup for external-cavity THz generation.

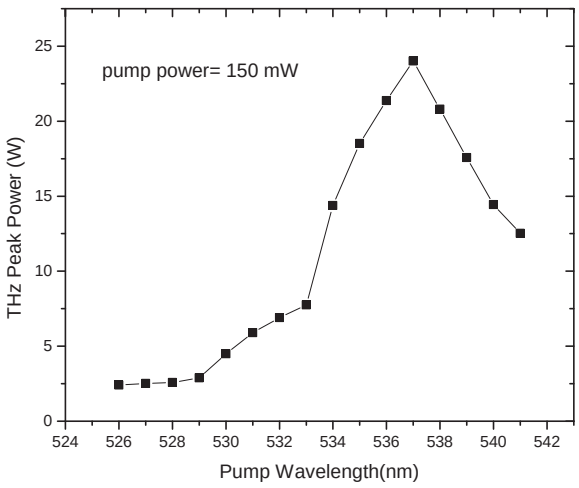

Fig. 16. THz peak power as a function of pump wavelength of OPO's, demonstrating QPM.

Each GaP plate used in our experiment has a thickness of 663 μm and a diameter of 48.5 mm. It was cut and polished on two (110) facets. The reflectivity from each GaP plate is about 20%, which is insufficient for being used as an output coupler. In order to reach a sufficiently high reflectivity, we stacked up to eight plates. While stacking, we alternatively rotated every the other plate to achieve QPM for the THz generation. We set the pump wavelength to one value within the range of 526-541 nm and measured the THz output power generated by the 8 pieces. We then set the pump wavelength to a different value and measured the output power again. According to Fig. 16, the THz output power reaches an optimal value at 537 nm (10 Hz, 5 ns), corresponding to the peak power of 24 W at the pump power of 150 mW. This is due to the reason that the QPM condition for the THz generation can be achieved for the set of the dual-signal wavelengths dictated by the pump wavelength of 537 nm and QPM for the OPO. When we set the pump to a value being different from 537 nm, the dual-signal wavelengths are shifted due to the QPM for the OPO, resulting in the change in the THz output wavelength.

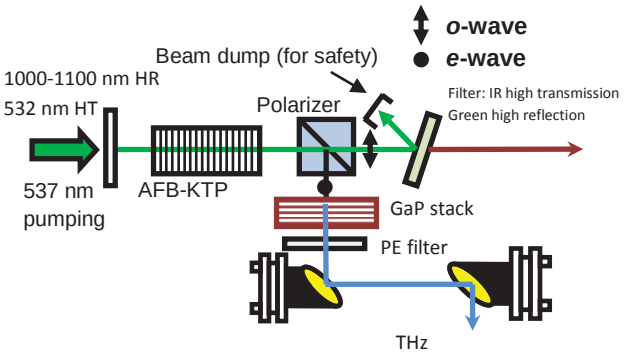

Fig. 17. Experimental setup for intracavity THz generation.

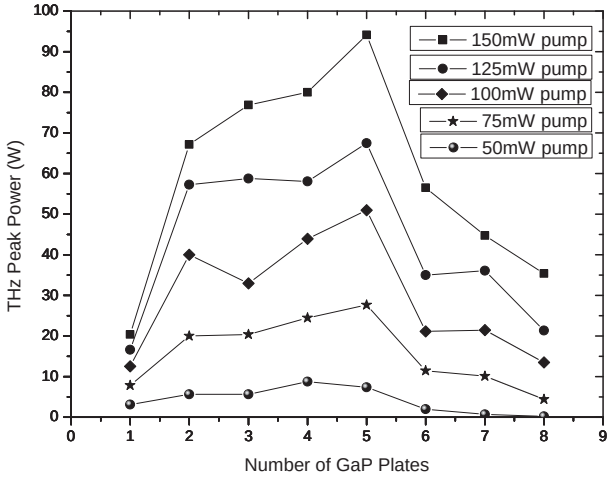

Fig. 18. THz power dependence on number of GaP plates.

For the intracavity THz generation, we set the pump wavelength to 537 nm such that the QPM condition for the THz generation is satisfied. We removed the HR output coupler for the dual-idler beams, see Fig. 17. Meanwhile, the stacked GaP plates were moved closer to the polarizer. It was well aligned for being used as an output coupler for the dual signals. As a result, the signals were resonated in the cavity consisting of the back reflector on the left side and the stacked GaP plates. The THz radiation was generated by the stacked GaP plates. This frequency-mixing process is another scheme for the intracavity THz generation, similar to Ref. [19]. We measured the THz output power as we set the pump power to five different values and set the number of the plates to the different values within 1-8, see Fig. 18. At the pump power of 50 mW, the highest output power was reached for four plates. However, for the pump powers of > 50 mW, the THz output power reached optimal values for five plates. At the pump power of 150 mW, the total THz power was measured to be about 188 W. Compared with the external-cavity [7], this power is a factor of 5 higher.

VI. Demonstration of THz interference

In this Section, we summarize our result following the observation of the THz interference. By mixing three nearly-even-spaced optical frequencies generated by coupled OPO's based in

KTP stacks and bulk KTP in a nonlinear medium, we demonstrate the coherent interference of the THz waves.

The experimental setup is shown in Fig. 19. This setup is different from the previous one. Indeed, we have inserted a half-wave plate between the polarizer and the GaSe crystal. To generate multiple THz wavelengths from the output beams of the coupled OPO's, the idler beam consisting three infrared wavelengths was first sent through a half-wave plate by the rotation by 45º to satisfy the polarization requirement, and then delivered onto a GaSe crystal. The adhesive-free-bonded (AFB) stacks [6] consist of 20 x-cut KTP plates, each of which has a thickness of 1.19 mm. The KTP stack composite has a clear aperture of 5.6 mm×10.5 mm. When the z axes of the KTP plates were periodically switched, they were bonded together via the AFB technique to form a strong composite such that the quasi-phase matching condition ($\Delta kl = \pm\pi$) is achieved for the OPO's. As a result, a single pair of the signal and idler frequencies is split into two signal wavelengths and two idler wavelengths at each pump wavelength. Hence, we introduced the terminology of coupled OPO's to distinguish them from the conventional OPO in where only a single pair of the signal and idler frequencies is generated. Beside the composite, an x-cut bulk KTP crystal (5 mm×5 mm×20 mm) was placed inside the OPO cavity. Consequently, the third set of signal and idler wavelengths was generated. In addition, the bulk KTP crystal was mounted inside an oven such that this set of the wavelengths can be precisely tuned by adjusting its temperature. The two cavity mirrors both have high-reflection coating in the range of 1000-1100 nm. The input mirror is coated for reaching the high transmittance at 532 nm (i.e. the pump wavelength of the OPO). To ensure the oscillations taking place only at three signal wavelengths, a cubic polarizer was placed inside the cavity. It reflects almost all of the *e*-polarized signal beams (R > 99%) such that most of the signal powers stayed inside the cavity whereas the *o*-polarized idler beam was efficiently coupled out of the cavity.

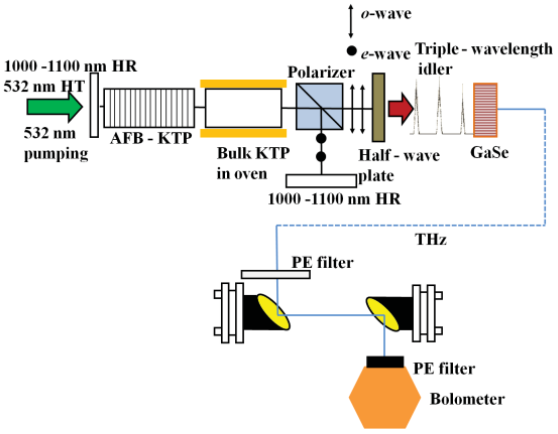

Fig. 19. Experimental Setup to generate triple idler beam and THz output.

Fig. 20 illustrates the spectrum of the idler output measured at room temperature. According to Fig. 20, there are three peaks at the wavelengths of 1084.3nm, 1089.3nm, and 1094.3nm, respectively. This means that the wavelength generated by the bulk KTP crystal was located exactly in the middle between the two idler wavelengths generated by the composite. The two difference

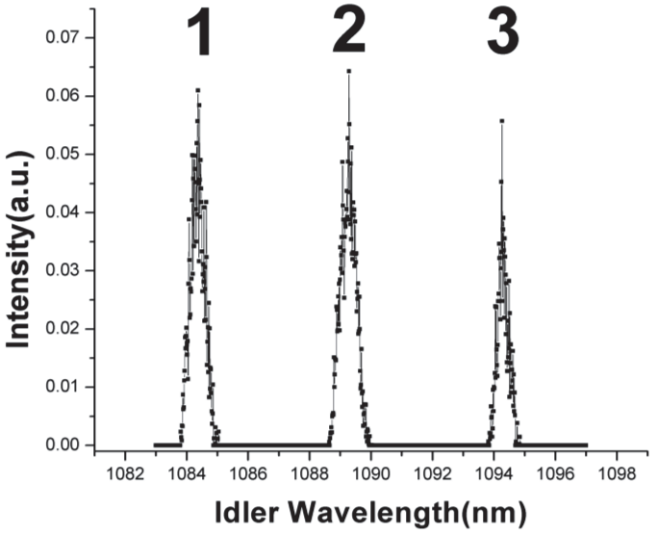

Fig. 20. Spectrum of the triple-wavelength idler beam measured at room temperature.

frequencies from such a set of the idler wavelengths can be calculated to be 1.2700 THz and 1.2584 THz, respectively. Due to the linewidths of the three idler peaks, the corresponding difference frequencies overlap in the THz spectrum. We measured the THz output power as a function of the phase-matching angle, see Fig. 21.

In Fig. 21, the peak at 119.88 μm (2.503 THz) originates from the mixing of the idler wavelengths labeled by 1 and 3 in Fig. 20. The stronger peak at 240.03μm (1.250THz) originates from the coherent interference of the two THz beams by mixing of those labeled by 1 and 2 and mixing of 2 and 3 in Fig. 20. As we increase the temperature of the bulk KTP crystal from 30 ºC to 45 ºC, the corresponding spectra of the THz output were measured by us, see Figs. 22(a)-(d). Fig. 22 illustrates a clear trend that when the temperature is increased, not only the strength of the interference peak decreases, but also the apparent peak is broadened. At the same time, the single peak at 119.88 μm remains unchanged. Such a trend indicates that we have indeed observed the coherent interference between the two THz beams having slightly different frequencies, which are generated by the GaSe crystal.

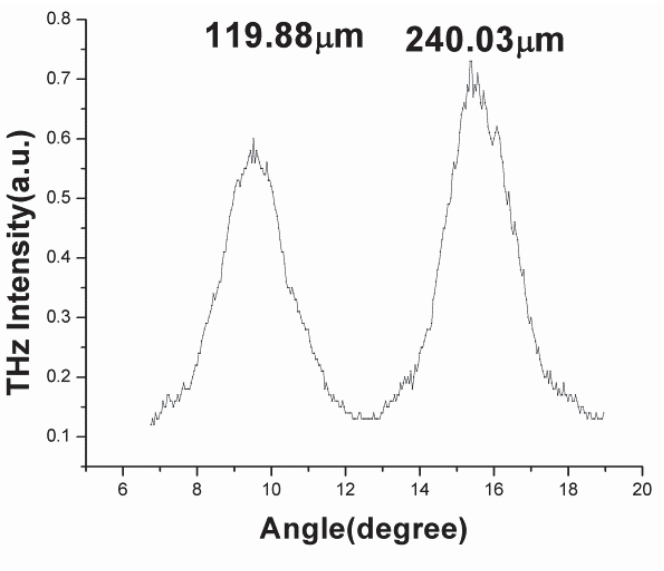

Fig. 21. Spectrum of the THz output beam as a function of phase-matching angle, generated by a GaSe crystal.

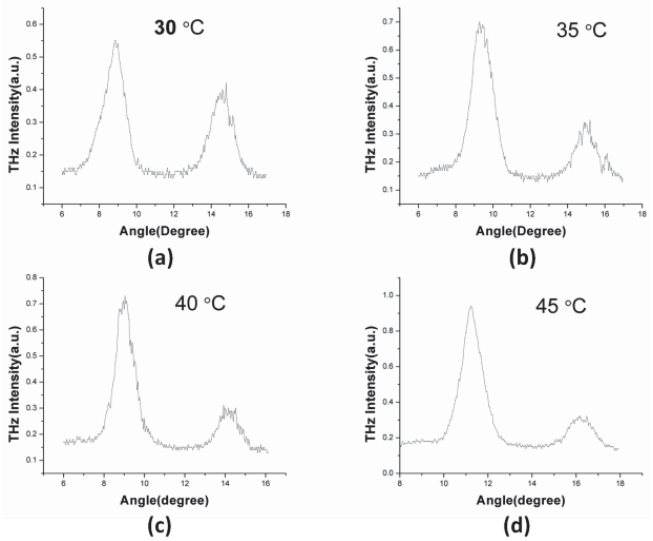

Fig. 22. Spectra of the THz output beam at different temperatures: a - 30 ºC, b - 35 ºC, c - 40ºC, d - 45 ºC.

VII. Conclusion

In conclusion, we have reviewed our progress on the applications of the coupled OPO's based on a composite consisting of the alternatively-rotated AFB KTP stacks. By using the phase-conjugate output generated by the composite, we have demonstrated that the spatial profile of the beam after propagating through the phase-distorted medium can be cleared up. In addition, we have restored the images after being blurred by the phase distortion. We have efficiently generated THz outputs by mixing the idler twins from the coupled OPO's. By using the alternatively-rotated GaP plates as an output coupler for the coupled OPO's, we have efficiently generated THz waves based on an intracavity configuration. By placing both the AFB KTP composite and a bulk KTP crystal in the same cavity, we have demonstrated the interference effects between the two THz beams generated by different pairs of the optical beams.

Our coupled OPO's possess unique properties compared with the conventional OPO. Indeed, the frequency separation within the idler twins or signal twins is insensitive to the fluctuations of the pump frequency and temperature.

Acknowledgements

We are indebted to X. Zou, P. Zhao, P. Hong, X. Lin, I. B. Zotova, X. Mu, H.-C. Lee, S. K. Meissner, and H. Meissner for making valuable contributions to some of the projects summarized in this article. This work has been partially supported by U.S. AFOSR.

References

[1]. U. Sharma, C. S. Kim, and J. U. Kang, "Highly stable tunable dual-wavelength Q-switched fiber laser for DIAL applications," IEEE Photon. Tech. Lett. **16**, 1277-1279 (2004).
[2]. R. Diaz, S. C. Chan, and J. M. Liu, "Lidar detection using a dual-frequency source," Opt. Lett. **31**, 3600-3602 (2006).
[3]. F. Ganikhanov, S. Carrasco, X. S. Xie, M. Katz, W. Seitz, and D. Kopf, "Broadly tunable dual-wavelength light source for coherent anti-Stokes Raman scattering microscopy," Opt. Lett. **31**, 1292-1294 (2006).
[4]. K. Miyamoto, and H. Ito, "Wavelength-agile mid-infrared (5-10 μm) generation using a galvano-controlled $KTiOPO_4$ optical parametric oscillator," Opt. Lett. **32**, 274-276 (2007).
[5]. H. Ito, K. Suizu, T. Yamashita, A. Nawahara, and T. Sato, "Random frequency accessible broad tunable terahertz-wave source using phase-matched 4-dimethylamino-N-methyl-4-stilbazolium tosylate crystal," Jap. J. Appl. Phys. **46**, 7321-7324 (2007).
[6]. X. Mu, H. Meissner, and H. C. Lee, "Optical parametric oscillations of 2 μm in multiple-layer bonded walk-off compensated KTP stacks," Opt. Lett. **35**, 387-389 (2010).
[7]. P. Zhao, S. Ragam, Y. J. Ding, I. B. Zotova, X. Mu, H.-C. Lee, S. K. Meissner, and H. Meissner, "Singly resonant optical parametric oscillator based on adhesive-free-bonded periodically inverted $KTiOPO_4$ plates: terahertz generation by mixing a pair of idler waves," Opt. Lett. **37**, 1283-1285 (2012).
[8]. X. Q. Zou, P. Zhao, P. Hong, X. Lin, Y. J. Ding, X. Mu, H.-C. Lee, S. K. Meissner, and H. Meissner, "Restoration of blurred images due to phase distortion based on polarization-insensitive phase conjugation in second-order nonlinear medium," Opt. Lett. **38**, 3054-3056 (2013).
[9]. P. Yeh, "Fundamental limit of the speed of photorefractive effect and its impact on device applications and material research," Appl. Opt. **26**, 602-604 (1987).
[10]. For a review, see various chapters in R. A. Fisher, ed., *Optical phase conjugation*, Academic, NY, 1983.
[11]. F. Devaux, E. Guiot, and E. Lantz, "Image restoration through aberrant media by optical phase conjugation in a type II three-wave mixing interaction," Opt. Lett. **23**, 1597-1599 (1998).
[12]. F. Devaux, G. le Tolguenec, and E. Lantz, "Phase conjugate imaging by type II parametric amplifcation," Opt. Commun. **147**, 309-312 (1998).
[13]. L. Lefort and A. Barthelemy, "Revisiting optical phase conjugation by difference-frequency generation," Opt. Lett. **21**, 848-850 (1996).
[14]. P. Zhao, Z. Liu, X. Lin, Y. J. Ding, X. Mu, H.-C. Lee, S. K. Meissner, and H. Meissner, "Polarization-Insensitive Optical Phase Conjugation Based on Adhesive-Free-Bonded Periodically-Inverted $KTiOPO_4$ Plates," CLEO 2013, CTu3E.7, June 9-14, 2013, San Jose, CA.
[15]. Y. Jiang, Y. J. Ding, and I. B. Zotova, "Power scaling of widely-tunable monochromatic terahertz radiation by stacking high-resistivity GaP plates," Appl. Phys. Lett. **96**, 031101 (2010).
[16]. Y. Jiang, D. Li, Y. J. Ding, and I. B. Zotova, "Terahertz generation based on parametric conversion: from saturation of conversion efficiency to back conversion," Opt. Lett. **36**, 1608-1610 (2011).
[17]. E. B. Petersen, W. Shi, A. Chavez-Pirson, N. Peyghambarian, and A. T. Cooney, "Efficient parametric terahertz generation in quasi-phase-matched GaP through cavity enhanced difference-frequency generation," Appl. Phys. Lett. **98**, 121119 (2011).

[18]. P. Zhao, X. Lin, Y. J. Ding, X. Mu, H.-C. Lee, S. Meissner, and H. Meissner, "Intracavity THz generation inside stacked GaP plates as output coupler of optical parametric oscillator," CLEO 2013, JTh2A.48.

[19]. P. Zhao, S. Ragam, Y. J. Ding, and I. B. Zotova, "Terahertz intracavity generation from output coupler consisting of stacked GaP Plates," Appl. Phys. Lett. **101**, 021107/1-3 (2012).M. V. Vasil´ev, V. Yu. Venediktov, and A. A. Leshchev, "Telescopic systems with dynamic nonlinear optical correction for distoritions," Quantum Electron. **31**, 1-15 (2001).